Electronic Supplementary Material (ESI) for ChemComm.

Supplementary information

Novel Synthetic Route for the Synthesis of Monodisperse β-$NaYF_4$:Ln^{3+} Micro-Nanocrystals from Layered Rare-Earth Hydroxides at ultra Low Temperature

Baiqi Shao, Qi Zhao, Yongchao Jia, Wenzhen Lv, Mengmeng Jiao, Wei Lü and Hongpeng You *[a]

Experimental Section

Preparation.$Y(NO_3)_3$, $Yb(NO_3)_3$, $Er(NO_3)_3$, and $Tm(NO_3)_3$ stock solution was obtained by dissolving corresponding Ln_2O_3 (99.99%) in dilute HNO_3 under heating with agitation until the final pH value was 4.0. All the other chemicals are of analytical grade and used without any purification.

In a typical synthesis, dilute ammonia (V/V=1:1) was introduced into 20 mL aqueous solution containing 1 mmoL $Y(NO_3)_3$ until pH=8 under magnetic stirring. The $Y_2(OH)_5(NO_3)\bullet 1.8H_2O$ white precipitation (with nanosheet morphology, about 7 nm in thickness) occurs immediately (corresponding XRD pattern, SEM image, TEM image, and TG curve are given in Figure S1. The value of n was calculated by the TG analysis.). After stirring for 10 min, 5 mL aqueous solution containing 4 mmol NaF was added into the above mixture and maintained at 50 ^{o}C for 3 h. Finally, the precipitation was collected and washed with deionized water and ethanol in turn several times and air-dried at 60 ^{o}C for 12 h. The $NaYF_4$:Yb^{3+},Er^{3+} and $NaYF_4$:Yb^{3+},Tm^{3+} were prepared by the similar process. For $NaYF_4$:20.8%Yb^{3+},1.78%Er^{3+}, 20 mL aqueous solution containing 0.78 mmoL $Y(NO_3)_3$, 0.2 mmoL $Yb(NO_3)_3$ and 0.02 mmoL $Er(NO_3)_3$ was stirred for 5 min, then dilute ammonia (V/V=1:1) was added into the above mixture solution until pH=8.0. After stirring for 10 min, 5 mL aqueous solution containing 4 mmol NaF was added into the above mixture and maintained at 50 ^{o}C for 3 h. Finally, the precipitation was collected and washed with deionized water and ethanol in turn several times and air-dried at 60 ^oC for 12 h.

Characterization. The phase structure of the as prepared products was characterized by powder X-ray diffraction with a D8 Focus diffractometer (Bruker, with Cu Kα radiation, λ=0.15406 nm) at a scanning rate of 10° min^{-1}. A field emission scanning electron microscope equipped with an energy-dispersive spectrometer (EDS) (FE-SEM, S-4800, Hitachi, Japan) was employed to inspected the morphology and size of the as prepared samples. Atomic force microscopy (AFM) measurements were performed with a microscopy (Seiko Instruments Industry Co.) The contents of Y, Yb, and Er were measured by a Leeman inductively coupled plasma (ICP) spectrometer. Transmission electron microscopy image were obtained using a JEOL-2010 transmission electron microscopy operating at 200 kV. Thermogravimetric analyses (TGA) were conducted on a thermal analysis instrument (SDT2960, TA Instruments, New Castle, DE) at 5 ^oC min^{-1} in an air flow of 100 mL min^{-1}. Upconversion photoluminescence spectra were recorded with a Hitachi F-4500spectrophotometer equipped with a 150 W xenon lamp as the excitation source, an external 980 nm diode laser and a R928P photomultiplier tube.

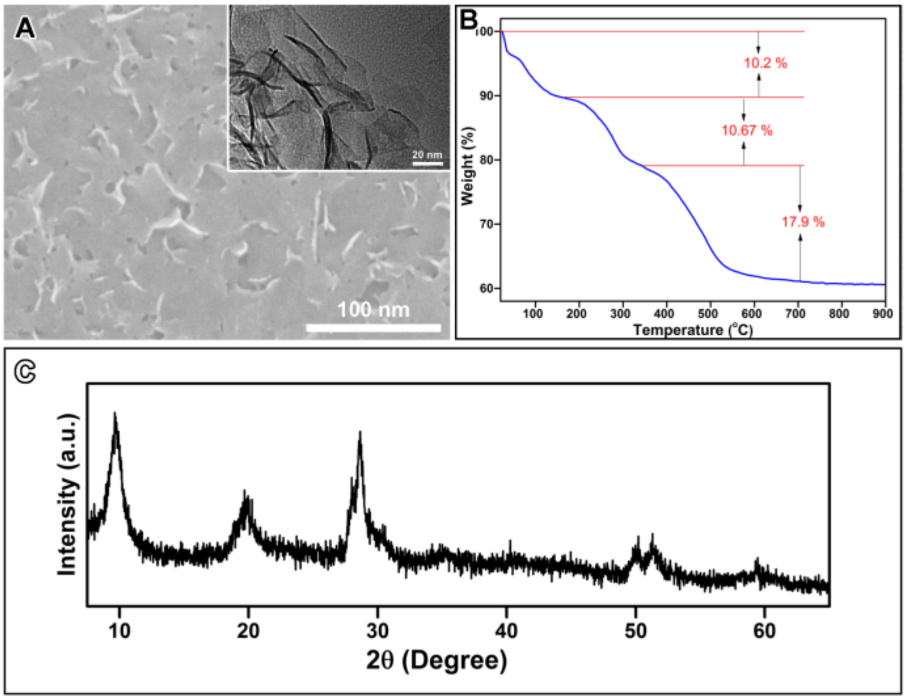

Fig. S1 SEM image (A), TEM image (inset panel), TG curve, and XRD pattern (C) of the as-prepared precursors. The XRD pattern can be indexed to $Y_2(OH)_5(NO_3)\bullet nH_2O$ (n is calculated to be about 1.8 by the TG analysis). The XRD pattern is consistent with the previous reports.[1, 2]

The TG curve displays three distinct weight losses, which is consistent with the results of other LRHs. The initial weight loss of 10.2 % before 180 °C corresponds to the removal of the cointercalated water molecules form the interlayer gallery. Such weight loss is calculated for 1.8 mmol of water molecular per chemical formula unit. The subsequent weight loss of 10.67 % (calculated weight loss is 10.6 %) is owing to the partial dehydroxylation of the hydroxide layers. The final weight loss of 17.9 % comes from the complete decomposition of the hydroxide layers to Y_2O_3 (calculated weight loss is 17.6 %).

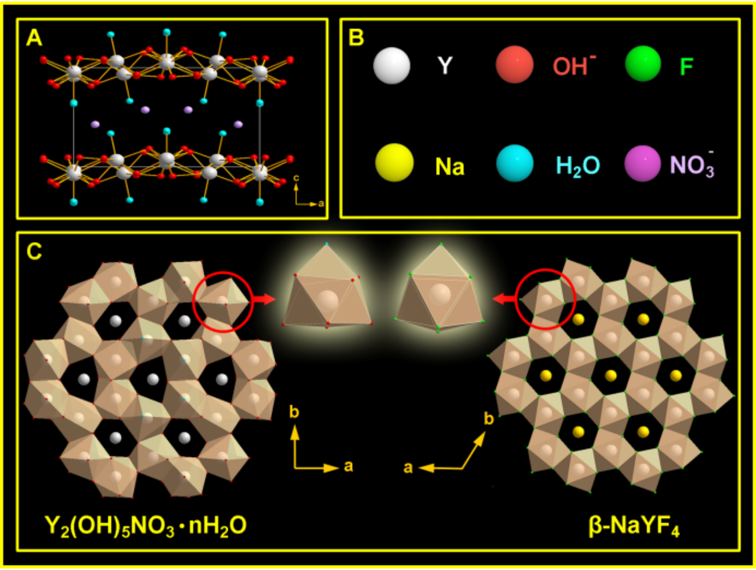

Fig. S2 Schematic representation of the crystallographic structure of the $Ln_2(OH)_5A•nH_2O$ viewed along the b-axis (A), the schemes of the ions and molecular (B), and the crystal structures of $Ln_2(OH)_5A•nH_2O$ and β-$NaYF_4$ viewed along c-axis (C).

For β-$NaYF_4$, there are three cation sites, a one-fold site for Y^{3+} (1a), a one-fold site for Na^+ and Y^{3+} (1f), and a two-fold site for Na^+ and vacancies (2h). The first two sites are nine-coordinated, forming an YF_9 trigonal prism with each vertical face bearing a pyramid. The YF_9 polyhedra linked to other three adjacent YF_9 polyhedra by edges along the {0001} plane forming a 2D crystal network of polyhedra with hexagonal tunnel structure wherein the Na^+ ions are inserted. In LYH crystal structure, there exist three sites containing 8- and 9-coordination for Y^{3+} in the unit layer. The first 8-coordination type is surrounded by seven hydroxyls and one water molecule, forming a distorted YO_8 dodecahedron. While the other two 9-coordination types are surrounded by eight hydroxyls and one water molecule, forming a YO_9 monocapped square antiprism. Intuitively, the YO_9 polyhedron can be viewed as a slightly distorted YF_9 polyhedron (Fig. 2), and the distance of Y-F bond (2.225-2.318 Å) is near to that of Y-O bond (HO···Y is 2.1-2.6 Å and H_2O···Y is 2.48 Å), which can greatly favor the ease of ion-exchange process. The YO_8 polyhedron is linked to two other YO_8 and four YO_9 polyhedra by edges, forming a 2D crystal network of polyhedra. Such crystal network of polyhedra is similar to that of the {0001} plane of β-$NaYF_4$ except that the distorted hexagonal tunnels are inserted with Y^{3+} ions. Besides, the wide interlamellar distance (about 8.5 Å) of the LYH enables the diffusion of the external ions into the gallery, which could greatly accelerate ion-exchange and reduce the energy barrier.

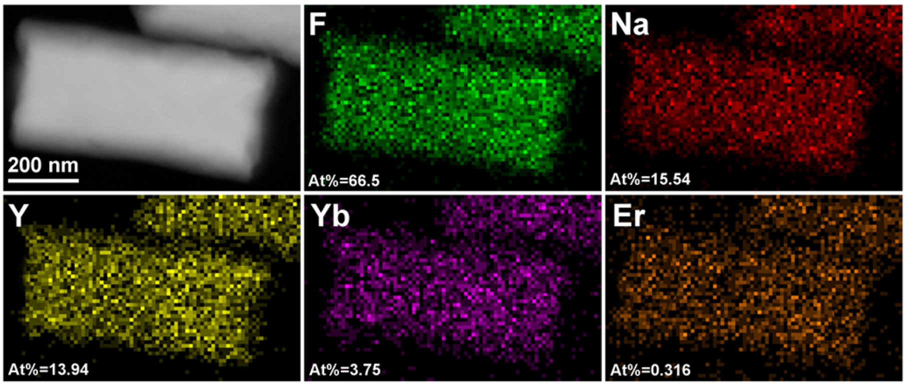

Fig. S3 High-angle annular dark-field scanning transmission electron microscopy (HADDF-STEM) of an individual β-$NaYF_4$:Yb,Er particle and elemental mapping images for each element, and the atomic molar ratio (At%) measured by ICP.

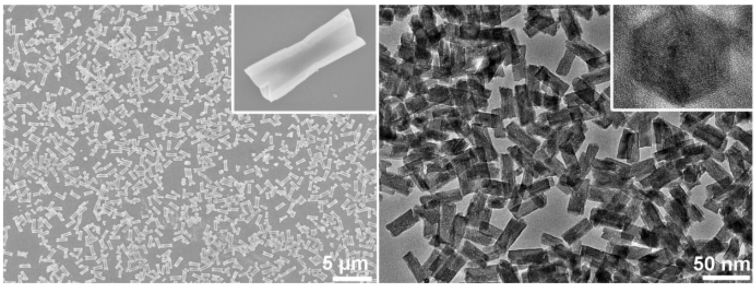

Fig. S4 SEM image of the products prepared with pH=7.0 (A) and TEM image of the products prepared with pH=10.0 (B).

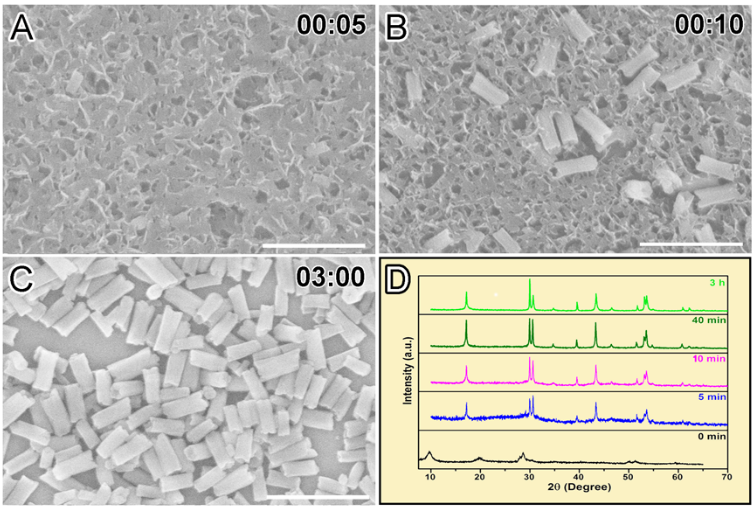

Fig. S5 SEM images of the samples at different reaction stages: (A) 5 min, (B) 10 min, (C) 3 h, and (D) corresponding XRD patterns. The time period began upon the adding of NaF. The scale bars are 1 μm.

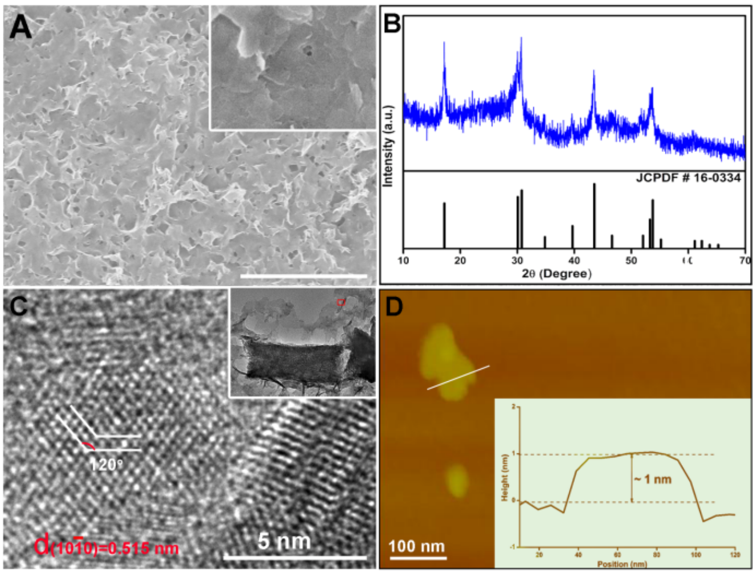

Fig. S6 SEM image (A) and XRD pattern (B) of the nanosheets prepared at 20 °C for 1 h. HRTEM image (C) and tapping-model AFM image with corresponding height profile (D) of the nanosheet collected with reaction time for 5 min at 50 °C.

Table 1. The Y/Yb/Er molar ratio in the LYH:Yb,Er precursor and $NaYF_4$:Yb,Er final product measured by ICP spectrometer.

	Y	**Yb**	**Er**
LYH:Yb,Er %	78.4	19.8	1.8
$NaYF_4$: Yb,Er %	77.4	20.8	1.78

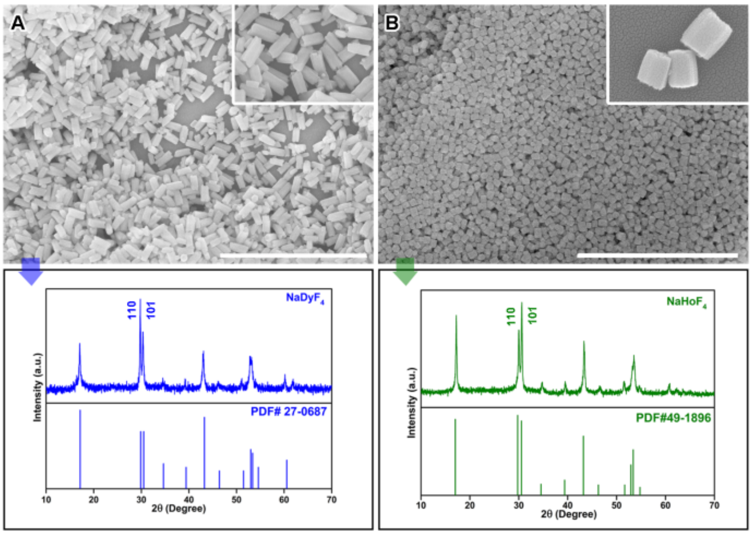

Fig. S7 SEM images and corresponding XRD patterns of the as-prepared $NaDyF_4$ (A) and $NaHoF_4$ (B) products. The scale bars are 5 μm.

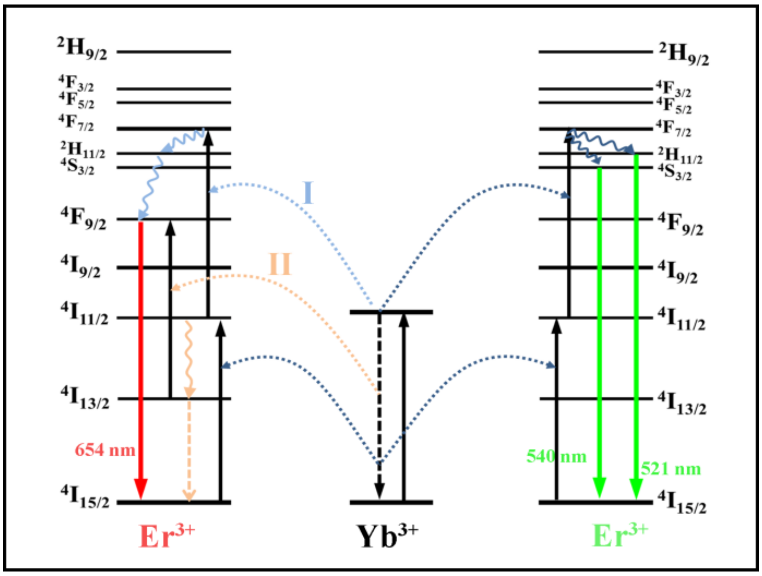

Fig. S8 Schematic illustration for the two-photon mechanism UC process of $NaYF_4$:20.8%Yb^{3+},1.78%Er^{3+} sample (left for red emission at 654 nm, right for green emissions at 521 and 540 nm).

The two-photon UC process for green emissions can be briefly described as follows.

$^2F_{5/2}(Yb^{3+}) + {}^4I_{15/2}(Er^{3+}) \rightarrow {}^2F_{7/2}(Yb^{3+}) + {}^4I_{11/2}(Er^{3+})$ (nonradiative energy transfer)

$^2F_{5/2}(Yb^{3+}) + {}^4I_{11/2}(Er^{3+}) \rightarrow {}^2F_{7/2}(Yb^{3+}) + {}^4I_{7/2}(Er^{3+})$ (nonradiative energy transfer)

$^4I_{7/2}(Er^{3+}) \rightarrow {}^2H_{11/2}(Er^{3+})$ or $^4S_{3/2}(Er^{3+})$ (nonradiative relaxation)

$^2H_{11/2}(Er^{3+})$ or $^4S_{3/2}(Er^{3+}) \rightarrow {}^4I_{15/2}(Er^{3+})$ (521 and 540 nm green emissions, respectively)

While, for 654 nm red emission, the $^4F_{9/2}(Er^{3+})$ level could be populated by two ways (Figure 7, left part). The first possible way can be described by follows, I:

$^2F_{5/2}(Yb^{3+}) + {}^4I_{15/2}(Er^{3+}) \rightarrow {}^2F_{7/2}(Yb^{3+}) + {}^4I_{11/2}(Er^{3+})$ (nonradiative energy transfer)

$^2F_{5/2}(Yb^{3+}) + {}^4I_{11/2}(Er^{3+}) \rightarrow {}^2F_{7/2}(Yb^{3+}) + {}^4I_{7/2}(Er^{3+})$ (nonradiative energy transfer)

$^4I_{7/2}(Er^{3+}) \rightarrow {}^2H_{11/2}(Er^{3+}) \rightarrow {}^4F_{9/2}(Er^{3+})$ (nonradiative relaxation)

And the other possible way, II:

$^2F_{5/2}(Yb^{3+}) + {}^4I_{15/2}(Er^{3+}) \rightarrow {}^2F_{7/2}(Yb^{3+}) + {}^4I_{11/2}(Er^{3+})$ (nonradiative energy transfer)

$^4I_{11/2}(Er^{3+}) \rightarrow {}^4I_{13/2}(Er^{3+})$ (nonradiative relaxation)

$^2F_{5/2}(Yb^{3+}) + {}^4I_{13/2}(Er^{3+}) \rightarrow {}^2F_{7/2}(Yb^{3+}) + {}^4F_{9/2}(Er^{3+})$ (nonradiative energy transfer)

And the 654 nm red emission can be yield through the $^4F_{9/2}(Er^{3+}) \rightarrow {}^4I_{15/2}(Er^{3+})$ transition.

1. Q. Zhu, J.-G. Li, C. Zhi, X. Li, X. Sun, Y. Sakka, D. Golberg and Y. Bando, *Chem. Mater.*, 2010, **22**, 4204-4213.
2. S. A. Hindocha, L. J. McIntyre and A. M. Fogg, *J. Solid State Chem.*, 2009, **182**, 1070-1074.